sciendo

Int. J. of Applied Mechanics and Engineering, 2020, vol.25, No.4, pp.1-21
DOI: 10.2478/ijame-2020-0046

INFLUENCE OF HEAT GENERATION/ABSORPTION ON MIXED CONVECTION FLOW BEHAVIOUR IN THE PRESENCE OF LORENTZ FORCES IN A VERTICAL MICRO CIRCULAR DUCT HAVING TIME PERIODIC BOUNDARY CONDITIONS: STEADY PERIODIC REGIME

B. AINA* and S. ISA
Department of Mathematics, Federal University Gashua
Yobe State - NIGERIA
E-mails: ainavicdydx@gmail.com; sanimath@yahoo.com

The problem of mixed convection flow of a heat generating/absorbing fluid in the presence existence of Lorentz forces in a vertical micro circular subjected to a periodic sinusoidal temperature change at the surface has been studied taking the first-order slip and jump effects into consideration. The research analysis is carried out by considering a fully developed parallel flow and steady periodic regime. The governing equations, together with the constraint equations which arise from the definition of mean velocity and temperature, are written in a dimensionless form and mapped into equations in the complex domain. One obtains two independent boundary value problems, which provide the mean value and the oscillating term of the velocity and temperature distributions. These boundary value problems are solved analytically. A parametric study of some of the physical parameters involved in the problem is conducted. The results of this research revealed that the magnetic field has a damping impact on the flow and results in decreases in fluid velocity for both air and water. Furthermore, the presence of the heat generation parameter is seen to enhance the temperature distribution and this is reflected as an increase in the magnitude of the oscillation dimensionless velocity, whereas in the presence of heat absorption a reversed trend occurs.

Key words: mixed convection, micro circular duct, Lorentz forces, heat generation/absorption, slip and jump, time - periodic.

1. Introduction

The study of convection flow and heat transfer containing volumetric heat generation are associated with large temperature difference and this is often encountered in many practical problems such as in spent fuel storage, in thermal control of space vehicles, in combustion chamber liners, in blading and casting of gas turbines, in fire and combustion modelling, in post accident heat removal, in high-performance insulation for buildings and in engine cooling system such as heat absorption in a car radiator. A good amount of literature is available on the influence of internal heat generation/absorption on flows. Records of such investigations can be found in the works of [1-10]. Jha *et al.* [11] examines the effect of a generating/absorbing fluid flow through a saturated porous medium filled in a vertical tube having time-periodic boundary condition on the surface of the tube. Jha and Ajibade [12] studied fully developed convection between two infinite vertical parallel plate with steady-periodic temperature regime in the presence of temperature-dependent heat absorption/generation. Jha and Aina [13] investigated the flow and heat transfer characteristics of a fully developed mixed convection flow of an electrically conducting, heat generating/absorbing fluid in a vertical tube due to periodic temperature variation on the vertical tube surface in the presence of a transverse magnetic field.

Recently, the effects of buoyancy on steady-periodic flows phenomenon have received considerable attention during the last two decades owing to the importance in technological applications, for instance, the

* To whom correspondence should be addressed

thermal control of electric resistors in alternating current or the development of heat-exchange enhancement techniques based on flows with time-oscillating mass rates. Numerous theoretical investigations have been carried out on the influence of periodic heating on flows in the past decade [14-23]. Barletta and Rossi di Schio [24] investigated the convection in circular duct with time-periodic boundary conditions. Makinde [25] carried out analysis of Non-Newtonian reactive flow in a cylindrical pipe. Chinyoka and Makinde [26] studied the transient flow of a reactive viscosity third grade fluid through a cylindrical pipe with buoyancy effects. Also, Chinyika *et al.* [27] presented theoretical studied on entropy analysis of unsteady magnetic flow through a porous pipe with buoyancy effects. Singh and Makinde [28] investigated axisymmetric slip flow on a vertical cylinder with heat transfer. Recently, Jha and Aina [29] studied the fully developed mixed convection flow in a vertical pipe having a time periodic boundary condition in the presence of a transverse magnetic field.

On the other hand, studies on micro-electro-mechanical system (MEMS) and nano-electrical-mechanical systems (NEMS) are getting more popular since the fluid is widely used in the design of micro-devices such as micro-motors, micro-sensors, micro-mechanical gyroscopes, micro-pumps, micro valves, micro-rockets, micro-gas-turbines, micro-heat-exchangers, biological and chemical devices etc. Micro-channels are used to transport biological material such as protein, DNA, cells and embryos or to transport chemical samples and analyses. The advantage of micro-channels is due to their high surface to volume ratio and their small volume. The large surface to volume ratio increases the rate of heat and mass transfer that makes micro devices excellent tools. Flow in heat transfer and chemical reactor devices are usually faster than those in biological devices and chemical analysis micro-devices. These applications have motivated scholars to understand the flow behaviours in these small systems to enhance the performance during the design process. Several researcher published articles about micro-channels and micro-tubes [30-35]. Recently, Jha and Aina [36] investigate fully developed mixed convection flow in the steady-periodic regime for a Newtonian fluid in a vertical microtube. They reported that the oscillation amplitude of the dimensionless temperature, velocity and pressure drop are dependent on the frequency of heating, strength of rarefaction parameter, fluid–wall interaction parameter and Prandtl number of the working fluid. The purpose of the present work is to generalise the work of Jha and Aina [36] by considering a generating/absorbing fluid flow under as a magnetic field flow in a vertical circular microtube having time-periodic boundary condition on the surface of the microtube. Analytical solutions of the momentum and energy equations are derived in terms of modified Bessel's function of first kind.

2. Mathematical analysis

A fully developed mixed convection flow of a viscous, incompressible, and electrically conducting fluid in a vertical micro circular duct having a periodic variation of temperature with time is considered in the presence of a transverse magnetic field. The velocities are assumed to be in a range such that the flow is always laminar. The flow is assumed to be parallel so that the $X-$component $\boldsymbol{U}$ of the velocity vector $\boldsymbol{U}$ is non zero. The $X-$axis is the axial coordinate which is parallel to the gravitational acceleration g but with opposite direction while the $R-$axis is the axis in the radial direction. A uniform magnetic field B_0 is assumed to be acting perpendicular to the flow direction. We assume that the magnetic Reynolds number is very small, which corresponds to the negligibly induced magnetic field compared to the externally applied one. Furthermore, the effect of viscous dissipation in the fluid is neglected.

Since only the axial component of U is non-vanishing, the mass balance equation ensures that $\partial U/\partial X = 0,$ i.e. $U = U\left(R,t\right).$ It is assumed that the pipe surface at $R = R_0$ is kept at an oscillating temperature with time, namely

$$T\left(X,R_0,t\right) = T_1 + \Delta T\cos\left(\omega t\right). \tag{2.1}$$

Moreover, since the thermal boundary condition (2.1) does not yield any net fluid heating or cooling, heat transfer occurs only in the radial direction, so that

$$\frac{\partial T}{\partial X}=0 \tag{2.2}$$

i.e. $T=T(R,t)$. The prescribed mass flow rate is assumed to be stationary, therefore average velocity in a pipe cross section, defined as

$$U_0=\frac{2}{R_0^2}\int_0^{R_0} RU(R,t)\,dR, \tag{2.3}$$

is time-independent. The equation of state $\rho=\rho(T)$ is considered as linear

$$\rho=\rho_0\left[1-\beta(T-T_0)\right] \tag{2.4}$$

where T_0 is the reference temperature with respect to both the pipe cross section and to a period of time, namely

$$T_0=\frac{\omega}{\pi R_0^2}\int_0^{\frac{2\pi}{\omega}} dt\int_0^{R_0} RT(R,t)\,dR. \tag{2.5}$$

Since $\frac{\partial T}{\partial X}=0$, T_0 is a constant.

By using the Boussinesq approximation, the governing equation of the momentum of conducting fluid in the presence of the magnetic field is as follows

$$\frac{\partial U}{\partial t}=-\frac{1}{\rho_0}\frac{\partial P}{\partial X}+g\beta(T-T_0)+\frac{1}{\rho_0}\frac{\mu}{R}\frac{\partial}{\partial R}\left(R\frac{\partial U}{\partial R}\right)-\frac{\sigma B_0^2 U}{\rho_0} \tag{2.6}$$

where $P=p+g\rho_0 X$ is the difference between the pressure and the hydrostatic pressure. By differentiating both sides of Eq.(2.6) with respect to X, one obtains $\frac{\partial^2 P}{\partial X^2}=0$. This result implies an existence of a function $A(t)$ such that

$$\frac{\partial P}{\partial X}=-A(t). \tag{2.7}$$

Then, Eq.(2.6) can be rewritten as

$$\frac{\partial U}{\partial t}=\frac{1}{\rho_0}A(t)+g\beta(T-T_0)+\frac{1}{\rho_0}\frac{\mu}{R}\frac{\partial}{\partial R}\left(R\frac{\partial U}{\partial R}\right)-\frac{\sigma B_0^2 U}{\rho_0}. \tag{2.8}$$

The energy balance equation is given by

$$\frac{\partial T}{\partial t} = \frac{\alpha}{R}\frac{\partial}{\partial R}\left(R\frac{\partial T}{\partial R}\right) + \frac{Q_0\left(T_0 - T\right)}{\rho_0 C_\rho}. \tag{2.9}$$

The non-dimensional quantities used in the above equation are defined as

$$\theta = \frac{T - T_0}{\Delta T},\ r = \frac{R}{2R_0},\ u = \frac{U}{U_0},\ \eta = \omega t,\ \Omega = \frac{4R_0^2\omega}{\nu},\ \lambda = \frac{4R_0^2 A(t)}{\mu U_0},\ \mathrm{Re} = \frac{2RU_0}{\nu},$$
$$\mathrm{Gr} = \frac{8g\beta\Delta T R_0^3}{\nu^2},\ \xi = \frac{T_1 - T_0}{\Delta T},\ \mathrm{Pr} = \frac{\nu}{\alpha},\ M = \frac{\sigma B_0^2 4R_0^2}{\mu},\ H = \frac{Q_0 4R_0^2}{\alpha\rho_0 C_\rho}. \tag{2.10}$$

The physical quantities used in the above equations are defined in the nomenclature.

Substituting the dimensionless quantities defined in Eqs (2.8) and (2.9), the dimensionless momentum and energy equations are

$$\Omega\frac{\partial u}{\partial \eta} = \lambda + \frac{\mathrm{Gr}}{\mathrm{Re}}\theta + \frac{1}{r}\frac{\partial}{\partial r}\left(r\frac{\partial u}{\partial r}\right) - M^2 u, \tag{2.11}$$

$$\Omega\,\mathrm{Pr}\frac{\partial \theta}{\partial \eta} = \frac{1}{r}\frac{\partial}{\partial r}\left(r\frac{\partial \theta}{\partial r}\right) - H\theta. \tag{2.12}$$

The dimensionless boundary conditions for the present physical situation are as follows

$$u\left(\frac{1}{2},\eta\right) = -\beta_v Kn\left.\frac{\partial u}{\partial r}\right|_{r=\frac{1}{2}},\qquad \left.\frac{\partial u}{\partial r}\right|_{r=0} = 0, \tag{2.13}$$

$$\theta\left(\frac{1}{2},\eta\right) = \xi + \cos(\eta) - \beta_v Kn\ln\left.\frac{\partial \theta}{\partial r}\right|_{r=\frac{1}{2}},\qquad \left.\frac{\partial \theta}{\partial r}\right|_{r=0} = 0 \tag{2.14}$$

where

$$\beta_v = \frac{2-\sigma_v}{\sigma_v},\qquad \beta_t = \frac{2-\sigma_t}{\sigma_t}\frac{2\gamma_s}{\gamma_s + 1}\frac{1}{\mathrm{Pr}},\qquad Kn = \frac{\lambda}{2R_0},\qquad \ln = \frac{\beta_t}{\beta_v}.$$

Referring to the values of σ_v and σ_t given in Eckert and Drake [25] and Goniak and Duffa [26], the value of β_v is near unity, and the value of β_t ranges from near 1 to more than 100 for actual wall surface conditions and is near 1.667 for many engineering applications, corresponding to $\sigma_v = 1$, $\sigma_t = 1$, $\gamma_s = 1.4$ and $\mathrm{Pr} = 0.71$ $(\beta_v = 1, \beta_t = 1.667)$.

From Eqs (2.3) and (2.5), the following two constraint equations in dimensionless form are

$$\int_0^{\frac{1}{2}} ru(r,\eta)\,dr = \frac{1}{8}, \tag{2.15}$$

$$\int_0^{2\pi} d\eta \int_0^{\frac{1}{2}} r\theta(r,\eta)\,dr = 0\,. \tag{2.16}$$

The fanning friction factor is defined as

$$f = \frac{2\tau_\omega}{\rho_0 U_0^2} = -\frac{2}{\mathrm{Re}}\frac{\partial u}{\partial r}\bigg|_{r=\frac{1}{2}}. \tag{2.17}$$

By differentiating with respect to η both sides of the integral constraint on $u(r,\eta)$ expressed in Eq.(2.15), we have

$$\int_0^{\frac{1}{2}} r\frac{\partial u(r,\eta)}{\partial \eta}\,dr = 0\,. \tag{2.18}$$

Multiplying both sides of the momentum equation in Eq.(2.11) by (r) and integrating with respect to r in the interval $\left[0,\frac{1}{2}\right]$, one obtains

$$\int_0^{\frac{1}{2}} \Omega r\frac{\partial u}{\partial \eta}\,dr = \lambda\int_0^{\frac{1}{2}} r\,dr + \frac{\mathrm{Gr}}{\mathrm{Re}}\int_0^{\frac{1}{2}} r\theta(r,\eta)\,dr + \int_0^{\frac{1}{2}} \frac{\partial}{\partial r}\left(r\frac{\partial u}{\partial r}\right)dr - M^2\int_0^{\frac{1}{2}} ru(r,\eta)\,dr\,, \tag{2.19}$$

which gives

$$f\,\mathrm{Re} = -2\frac{\partial u}{\partial r}\bigg|_{r=\frac{1}{2}}, \tag{2.20}$$

$$= \frac{\lambda}{2} - \frac{M^2}{2} + 4\frac{\mathrm{Gr}}{\mathrm{Re}}\int_0^{\frac{1}{2}} r\theta(r,\eta)\,dr\,. \tag{2.21}$$

3. Analytical solution: velocity and temperature distribution

In the steady periodic regime, the momentum and energy balance Eqs (2.11) and (2.12), together with the boundary conditions (2.13) and (2.14) and the constraints (2.15) and (2.16) can be solved analytically by considering the function $u(r,\eta)$, $\theta(r,\eta)$ and $\lambda(\eta)$ as the real parts of three complex valued functions, namely

$$u(r,\eta) = \Re e\left[u^*\left((r,\eta)\right)\right],$$

$$\theta(r,\eta) = \Re e\left[\theta^*\left((r,\eta)\right)\right], \tag{3.1}$$

$$\lambda(\eta) = \Re e\left[\lambda(\eta)\right].$$

On the account of Eqs (2.11) - (2.16), the complex valued functions $u^*(r,\eta)$, $\theta^*(r,\eta)$ and $\lambda^*(\eta)$ must be the solution to the boundary value problem

$$\Omega\frac{\partial u^*}{\partial \eta} = \lambda^* + \frac{\mathrm{Gr}}{\mathrm{Re}}\theta^* + \frac{1}{r}\frac{\partial}{\partial r}\left(r\frac{\partial u^*}{\partial r}\right) - M^2 u^*, \tag{3.2}$$

$$\Omega\,\mathrm{Pr}\frac{\partial \theta^*}{\partial \eta} = \frac{1}{r}\frac{\partial}{\partial r}\left(r\frac{\partial \theta^*}{\partial r}\right) - H\theta^*, \tag{3.3}$$

$$u^*\left(\frac{1}{2},\eta\right) = -\beta_v Kn\left.\frac{\partial u^*}{\partial r}\right|_{r=\frac{1}{2}}, \quad \left.\frac{\partial u^*}{\partial r}\right|_{r=0} = 0, \tag{3.4}$$

$$\theta^*\left(\frac{1}{2},\eta\right) = \xi + e^{i\eta} - \beta_v Kn\ln\left.\frac{\partial \theta^*}{\partial r}\right|_{r=\frac{1}{2}}, \quad \left.\frac{\partial \theta^*}{\partial r}\right|_{r=0} = 0, \tag{3.5}$$

$$\int_0^{\frac{1}{2}} r u^*(r,\eta)\,dr = \frac{1}{8}, \tag{3.6}$$

$$\int_0^{2\pi} d\eta \int_0^{\frac{1}{2}} r\theta^*(r,\eta)\,dr = 0. \tag{3.7}$$

Therefore, one has

$$u^*(r,\eta) = u_a^*(r) + \frac{\mathrm{Gr}}{\mathrm{Re}}u_b^*(r)\exp(i\eta),$$

$$\theta^*(r,\eta) = \theta_a^*(r) + \theta_b^*(r)\exp(i\eta), \tag{3.8}$$

$$\lambda^*(\eta) = \lambda_a^* + \frac{\mathrm{Gr}}{\mathrm{Re}}\lambda_b^*\exp(i\eta).$$

By substituting Eq.(3.8) into Eqs (3.2)-(3.5), one obtains two independent boundary value problems. The first boundary value problem is expressed as

$$\frac{1}{r}\frac{d}{dr}\left(r\frac{du_a^*}{dr}\right) - M^2 u_a^* + \lambda_a^* + \frac{\mathrm{Gr}}{\mathrm{Re}}\theta_a^* = 0,$$

$$\frac{1}{r}\frac{d}{dr}\left(r\frac{d\theta_a^*}{dr}\right)-H\theta_a^*=0\,,$$

$$u_a^*\left(\frac{1}{2}\right)=-\beta_v Kn\left.\frac{du_a^*}{dr}\right|_{r=\frac{1}{2}},\qquad \left.\frac{du_a^*}{dr}\right|_{r=0}=0\,,$$

$$\theta_a^*\left(\frac{1}{2}\right)=\xi-\beta_v Kn\ln\left.\frac{d\theta_a^*}{dr}\right|_{r=\frac{1}{2}},\qquad \left.\frac{d\theta_a^*}{dr}\right|_{r=0}=0\,, \tag{3.9}$$

$$\int_0^{\frac{1}{2}} ru_a^*(r)\,dr=\frac{1}{8},$$

$$\int_0^{\frac{1}{2}} r\theta_a^*(r)\,dr=0\,,$$

while the second order is given by

$$\frac{1}{r}\frac{d}{dr}\left(r\frac{du_b^*}{dr}\right)-M^2u_b^*-i\Omega u_b^*+\lambda_b^*+\theta_b^*=0\,,$$

$$\frac{1}{r}\frac{d}{dr}\left(r\frac{d\theta_b^*}{dr}\right)-i\Omega\,\mathrm{Pr}\,\theta_b^*-H\theta_b^*=0\,,$$

$$u_b^*\left(\frac{1}{2}\right)=-\beta_v Kn\left.\frac{du_b^*}{dr}\right|_{r=\frac{1}{2}},\qquad \left.\frac{du_b^*}{dr}\right|_{r=0}=0\,,$$

$$\theta_b^*\left(\frac{1}{2}\right)=1-\beta_v Kn\ln\left.\frac{d\theta_b^*}{dr}\right|_{r=\frac{1}{2}},\qquad \left.\frac{d\theta_b^*}{dr}\right|_{r=0}=0\,, \tag{3.10}$$

$$\int_0^{\frac{1}{2}} ru_b^*(r)\,dr=0\,,$$

$$\int_0^{\frac{1}{2}} r\theta_b^*(r)\,dr=0$$

.

By employing the constraint on $\theta_a^*(r)$ yields $\xi=0$, i.e., $T=T_0$ the solution of Eq.(30) is

$$\theta_a^*(r) = 0\,,$$

$$u_a^*(r) = \frac{\lambda_a^*}{M^2}\left[\frac{I_0(0.5D_1) + \beta_v KnD_1 I_1(0.5D_1) - I_1(rD_1)}{I_0(0.5D_1) + \beta_v KnD_1 I_1(0.5D_1)}\right], \tag{3.11}$$

$$\lambda_a^* = \frac{M^2 D_1 I_0(0.5D_1) + \beta_v KnD_1 I_1(0.5D_1)}{\{D_1 I_0(0.5D_1) + \beta_v KnD_1 I_1(0.5D_1)\} - 4I_0(0.5D_1)}\,,$$

while the solution of Eq.(3.10) is

$$\theta_b^*(r) = \frac{I_0(rD_2)}{I_0(0.5D_2) + \beta_v KnD_2 I_1(0.5D_2)}\,,$$

$$u_b^*(r) = \left(d_8 + d_7\lambda_b^*\right)I_0(rD_3) + \frac{\lambda_b^*}{D_3^2} + \frac{I_0(rD_2)}{\left(D_3^2 - D_2^2\right)I_0(0.5D_2) + \beta_v KnD_2 I_1(0.5D_2)}\,, \tag{3.12}$$

$$\lambda_b^* = \frac{-d_{13} - d_{10}}{d_{11} + d_{12}}$$

where

$$D_1 = M\,, \qquad D_2 = \sqrt{i\Omega\,\mathrm{Pr} + H} \qquad \text{and} \qquad D_3 = \sqrt{M^2 + i\Omega}\,.$$

The values of $d_1 - d_{13}$ are defined in the Appendix.
The fanning friction factor can be written as

$$f\,\mathrm{Re} = \mathrm{Re}\left[f_a^*\,\mathrm{Re} + f_b^*\frac{\mathrm{Gr}}{\mathrm{Re}}\exp(i\eta)\right] \tag{3.13}$$

where f_a^* and f_b^* are respectively given by

$$f_a^*\,\mathrm{Re} = -2\left.\frac{du_a^*}{dr}\right|_{r=\frac{1}{2}} \quad f_b^*\,\mathrm{Re} = -2\left.\frac{du_b^*}{dr}\right|_{r=\frac{1}{2}}. \tag{3.14}$$

4. Results and discussion

In order to have a physical insight into the problem, we have written a MATLAB programme to compute and generate the graphs for the dimensionless velocity, dimensionless temperature, dimensionless pressure drop, and dimensionless friction factor. Some representative results are presented in the form of line graphs in Figures 1-19 to interpret the effects of these parameters. The negative value of H corresponds to the internal heating of the fluid, while the positive value corresponds to the internal cooling of the fluid.

Figures 1 and 2 depict the influence of the Lorentz force on the radial distribution of $\left|U_b^*\right|$ under the cases of a small value of dimensionless frequency $(\Omega = 0.5)$ and large value of dimensionless frequency

$(\Omega = 50)$. It is observed in Figs 1 and 2 that an increase in the value of Lorentz forces tends to slow down the movement of the fluid in the vertical micro circular duct. Physically speaking, the retarding effect of the magnetic force is strengthened with the increase in the Lorentz force. This increase in the Lorentz force decreases the thickness of the momentum boundary layer and induces a Lorentz force which opposes the fluid flow. The radial distribution of $\left|U_b^*\right|$ in Figs 3 and 4 has two local maximum, one local maxima on the circular micro-duct axis while the other close to the circular micro-duct surface. Further, the presence of a local minimum arises for $r \approx 0.3$. This local minimum is more evident in Fig.3 in the case of a small value of dimensionless frequency $(0 < \Omega < 2.0)$.

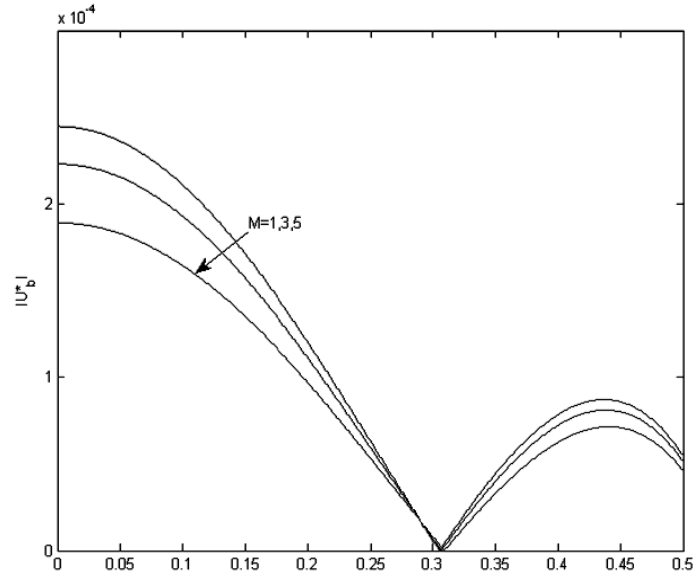

Fig.1. Radial distribution $\left|U_b^*\right|$ for different values of M with $\Omega = 0.5$, $H=0.5$, Pr=0.71, $\beta_v Kn = 0.05$, $In=1.667$.

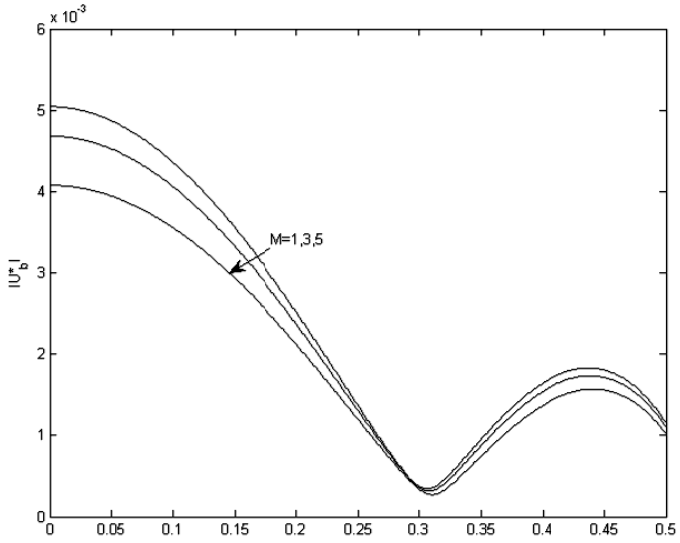

Fig.2. Radial distribution $\left|U_b^*\right|$ for different values of M with $\Omega = 50$, $H=0.5$, Pr=0.71, $\beta_v Kn = 0.05$, $In=1.667$.

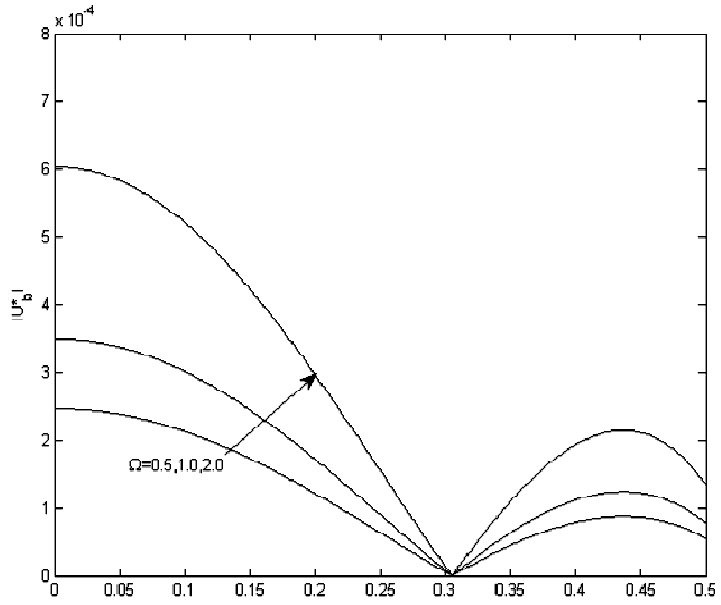

Fig.3. Radial distribution $\left|U_b^*\right|$ for different values of $\Omega\left(0.5 < \Omega < 2.0\right)$ with *M=0.5*, *H=0.5*, Pr=*0.71*, $\beta_v Kn = 0.05$, *In=1.667*.

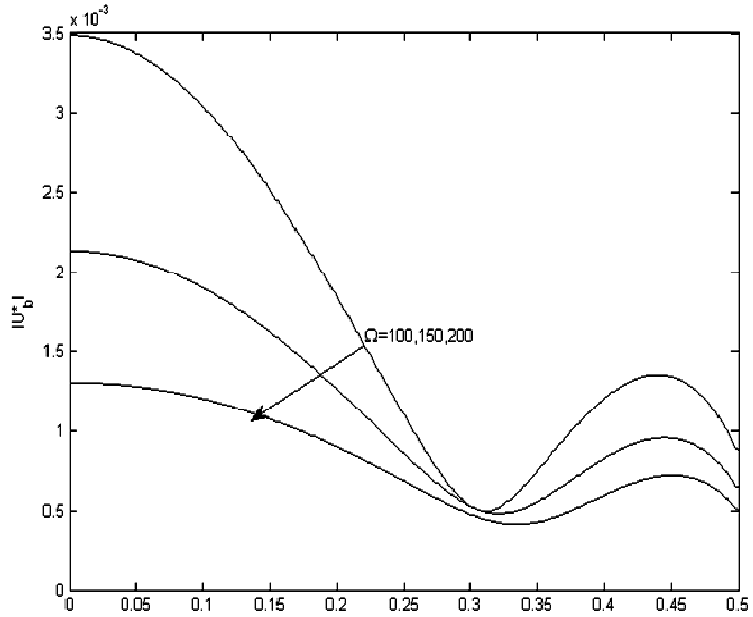

Fig.4. Radial distribution $\left|U_b^*\right|$ for different values of $\Omega\left(100 < \Omega < 200\right)$ with *M=0.5*, *H=0.5*, Pr=*0.71*, $\beta_v Kn = 0.05$, *In=1.667*.

Figures 5 and 6 illustrate the effect of the rarefaction parameter on radial distribution of $\left|U_b^*\right|$ for a small value of dimensionless frequency $\left(\Omega = 0.5\right)$ as well as a large value of dimensionless frequency $\left(\Omega = 50\right)$, respectively. It is observed for small value of dimensionless frequency that, increase in the

rarefaction parameter enhances the velocity slip for both air and water while the reverse is the case of a large value of dimensionless frequency. This result yields an observable increase in the fluid velocity.

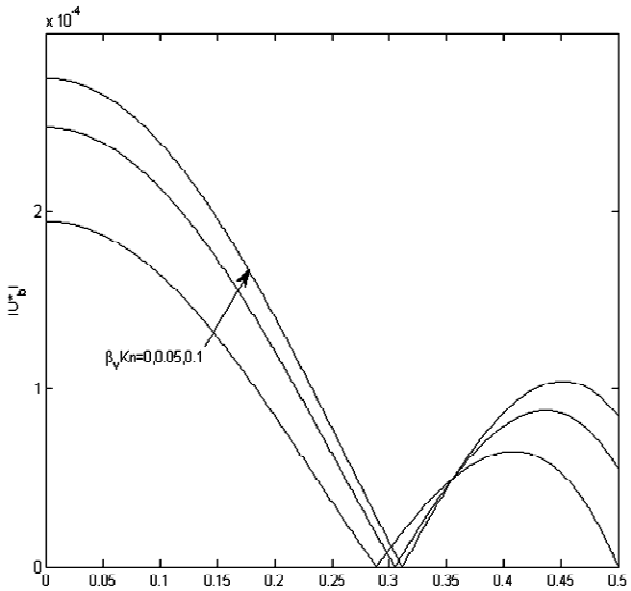

Fig.5. Radial distribution $\left|U_b^*\right|$ for different values of $\beta_v Kn$ with *M=0.5*, *H=0.5*, Pr=*0.71*, $\Omega = 0.5$, *In=1.667*.

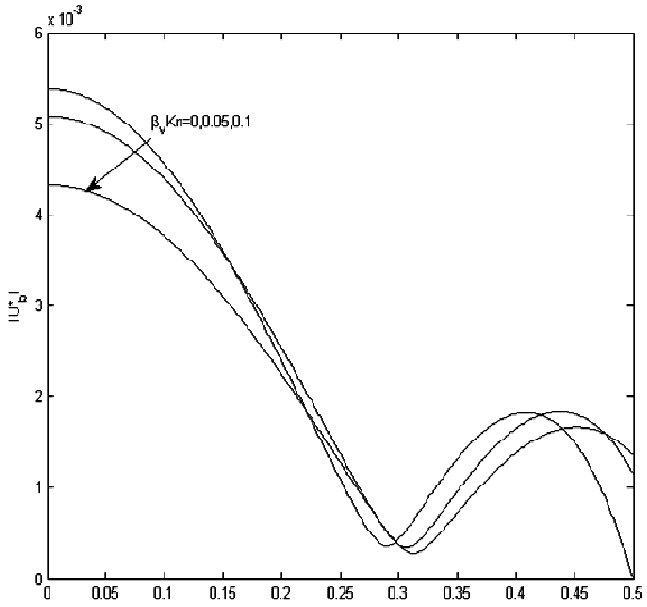

Fig.6. Radial distribution $\left|U_b^*\right|$ for different values of $\beta_v Kn$ with *M=0.5*, *H=0.5*, Pr=*0.71*, $\Omega = 50$, *In=1.667*.

The effect of the fluid wall interaction parameter on radial distribution of $\left|U_b^*\right|$ is shown in Figs 7 and 8. We observed for both small and large values of dimensionless frequency that the role of the fluid wall interaction parameter is to reduce the fluid velocity in the circular micro-duct. Furthermore, the effects of the

fluid wall interaction parameter on the radial distribution of $\left|U_b^*\right|$ become significant in the case of large values of dimensionless frequency.

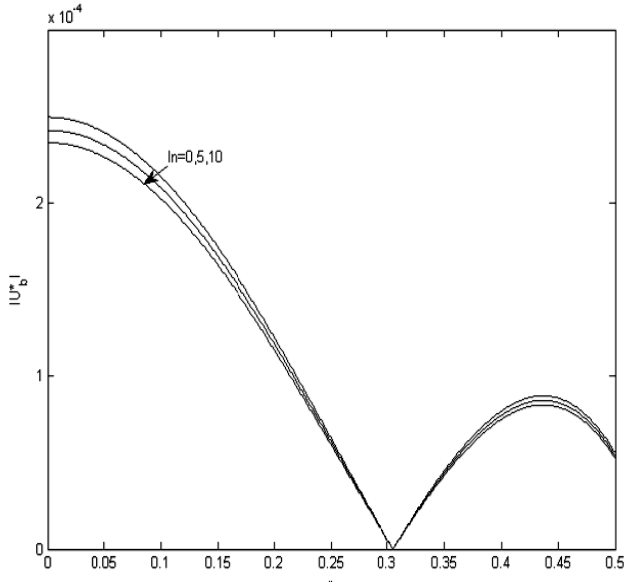

Fig.7. Radial distribution $\left|U_b^*\right|$ for different values of ln with *M=0.5*, *H=0.5*, Pr=*0.71*, $\Omega = 0.5$, $\beta_v Kn = 0.05$.

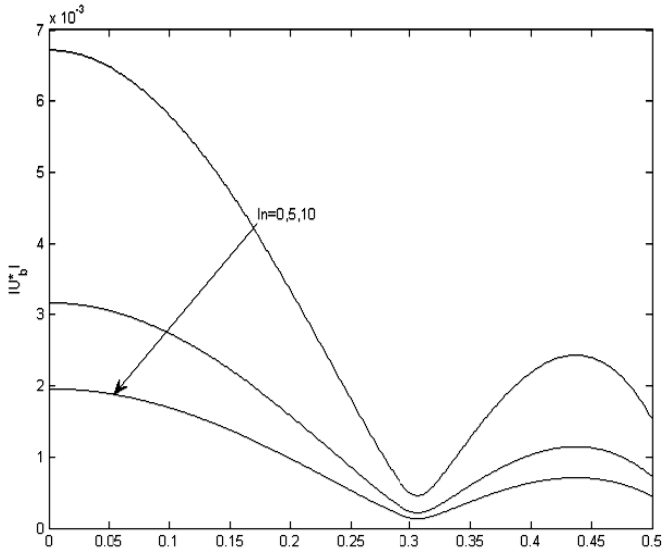

Fig.8. Radial distribution $\left|U_b^*\right|$ for different values of ln with *M=0.5*, *H=0.5*, Pr=*0.71*, $\Omega = 50$, $\beta_v Kn = 0.05$.

Figure 9 depicts the variation of radial distribution of $\left|U_b^*\right|$ versus the heat generation/absorption parameter. It is seen that an increase in the heat generation parameter in the range $(0 < \Omega < 2.0)$ increases the convectional current in the fluid while the reverse is the case of internal heating (Fig.10).

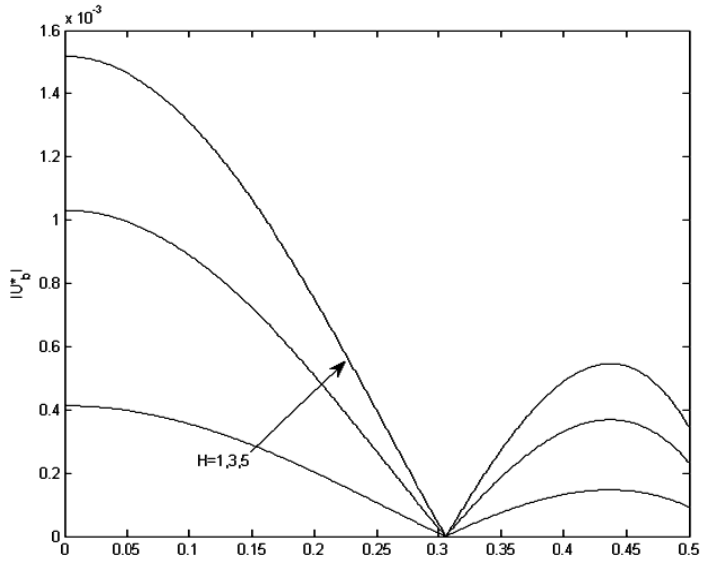

Fig.9. Radial distribution $\left|U_b^*\right|$ for different values of H with Pr=*0.71*, $\Omega = 0.5$, *In=1.667*, *M=0.5*, $\beta_v Kn$ *=0.05*.

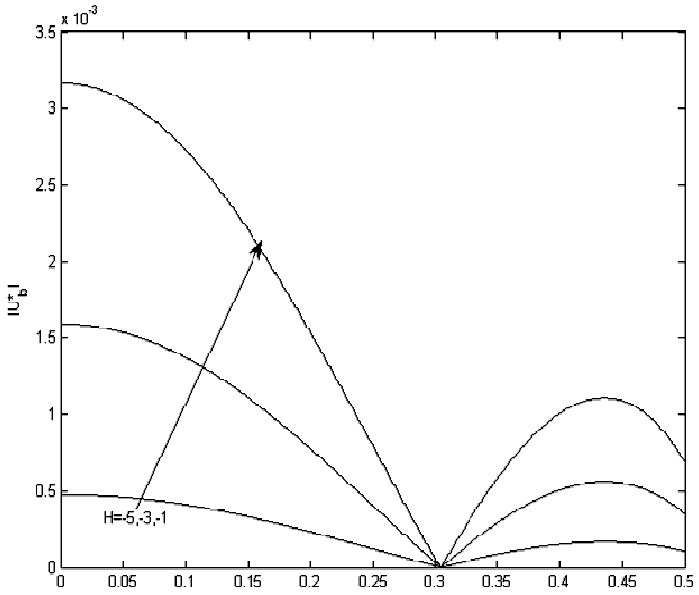

Fig.10. Radial distribution $\left|U_b^*\right|$ for different values of H (Negative) with Pr=*0.71*, $\Omega = 0.5$, *In=1.667*, *M=0.5*, $\beta_v Kn$ *=0.05*.

Figures 11 and 12 represents the influence of the rarefaction parameter and fluid wall interaction parameter on the radial distribution of $\left|\theta_b^*\right|$. These figures reveal that, increase in the rarefaction parameter as well as in the fluid wall interaction parameter leads to a reduction on radial distribution of $\left|\theta_b^*\right|$.

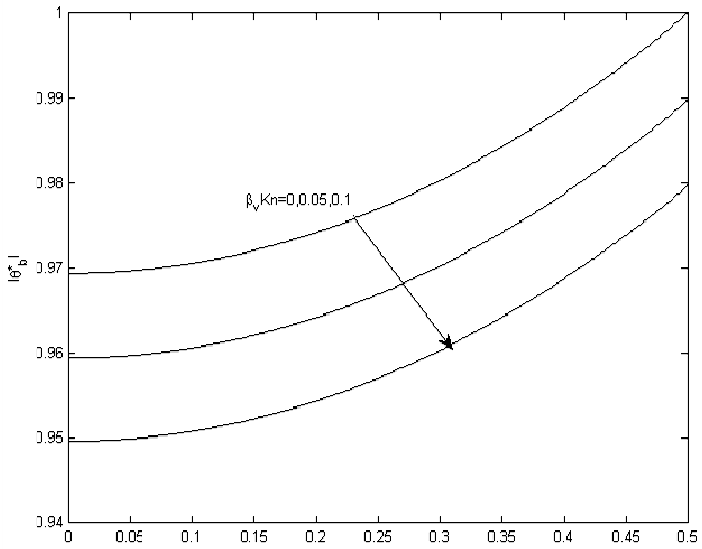

Fig.11. Radial distribution $\left|\theta_b^*\right|$ for different values of $\beta_v Kn$ with $\Omega = 0.5$, $In=1.667$, $H=0.5$.

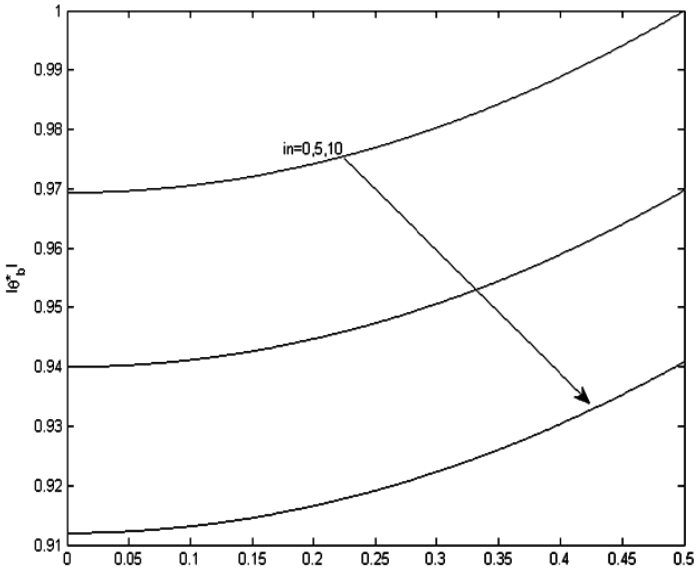

Fig.12. Radial distribution $\left|\theta_b^*\right|$ for different values of with $\Omega = 0.5$, $\beta_v Kn = 0.05$, $H=0.5$.

Figure 13 represents the radial variation of $\left|\theta_b^*\right|$ versus the heat generation/absorption parameter (H). It is evident that as the heat generation increases temperature also increases, while increasing the heat absorption decreases the temperature. This is physically true because heat generation causes an increase in the temperature distribution, while on the contrary, heat absorption decreases the temperature distribution.

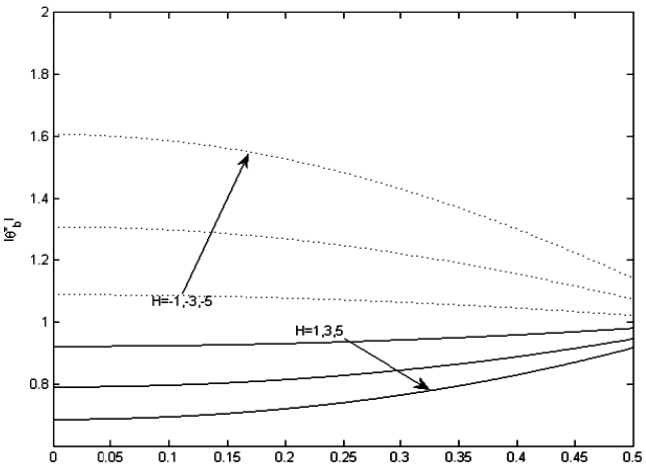

Fig.13. Radial distribution $\left|\theta_b^*\right|$ for different values of H with $\Omega = 0.5$, $\beta_v Kn = 0.05$, $In = 1.667$.

Figures 14 and 15 display the impacts of the Prandtl number and dimensionless frequency on the distribution of $\left|U_b^*\right|$ at the axis of the circular micro-duct $(r = 0)$ and near the circular micro-duct surface $(r = 0.4)$, respectively. These figures show that for any radial position there exists a dimensionless resonance frequency such that the oscillation amplitude of the dimensionless velocity distribution reaches a maximum. This resonance frequency is a function of the radial position as well as the Prandtl number. Figures 16 and 17 represent the distribution of $\left|U_b^*\right|$ for different values of the heat generation/absorption parameter at the axis of the circular micro-duct $(r = 0)$ and near the circular micro-duct surface $(r = 0.4)$, respectively. These figures revealed that at different radial positions, there exists a resonance frequency that gives a maximum oscillation amplitude of the dimensionless velocity. In addition, these figures show that an increase in heat generation leads to a reduction in the distribution of $\left|U_b^*\right|$.

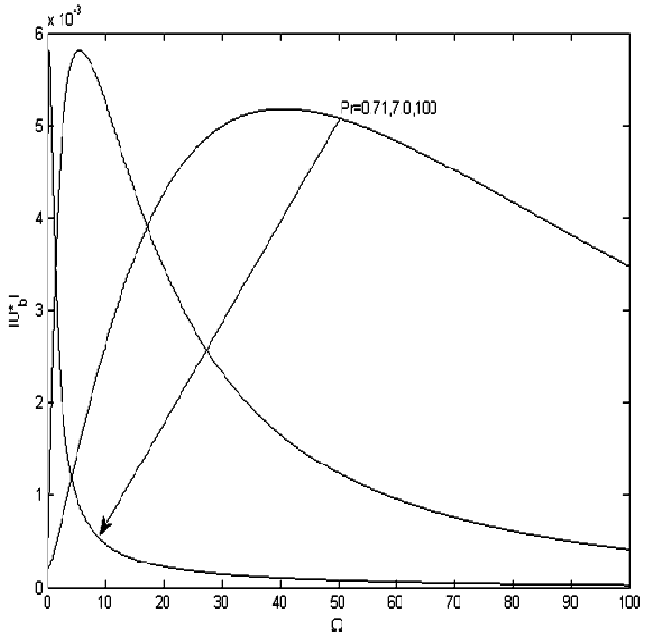

Fig.14. Distribution of $\left|U_b^*\right|$ versus Ω for different values of Pr with $\beta_v Kn = 0.05$, $H = 0.5$, $In = 1.667$, $r = 0.0$.

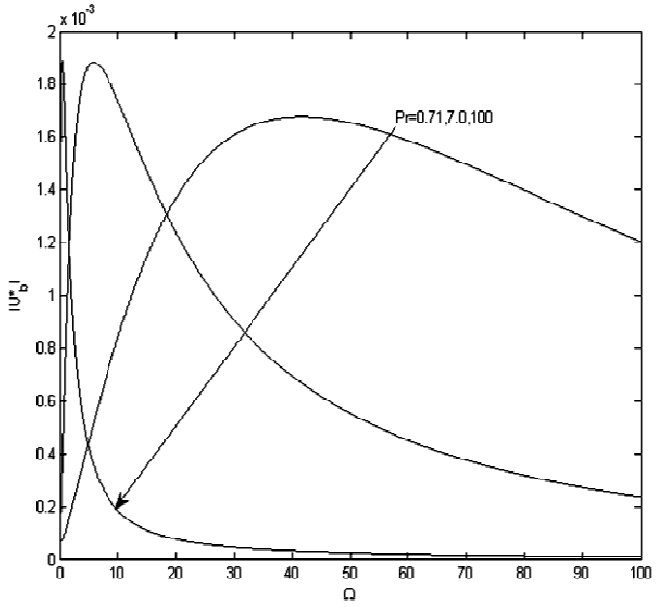

Fig.15. Distribution of $\left|U_b^*\right|$ versus Ω for different values of Pr with $\beta_v Kn = 0.05$, $H = 0.5$, $In = 1.667$, $r = 0.4$.

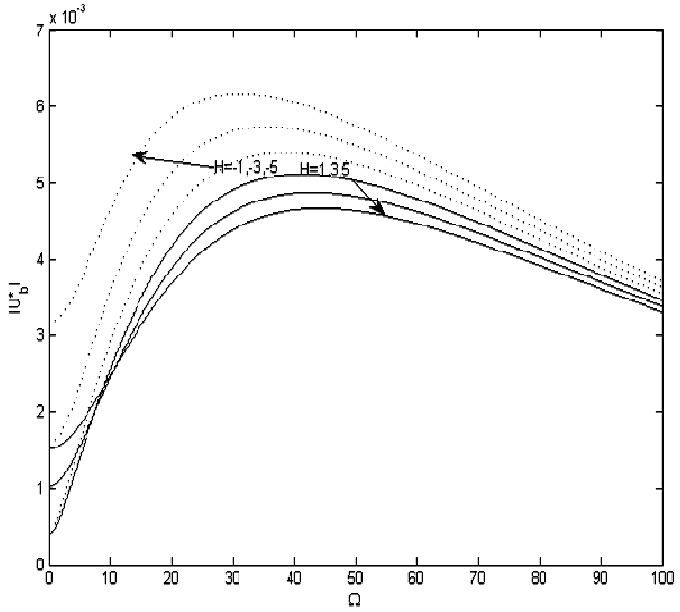

Fig.16. Distribution of $\left|U_b^*\right|$ versus Ω for different values of H with $\beta_v Kn = 0.05$, Pr$=0.71$, $In = 1.667$, $r = 0.0$.

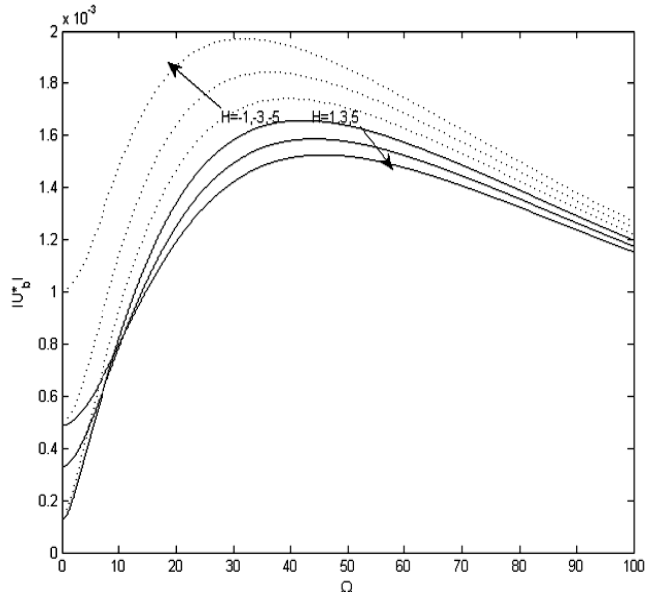

Fig.17. Distribution of $\left|U_b^*\right|$ versus Ω for different values of H with $\beta_v Kn = 0.05$, Pr=*0.71*, *In=1.667*, *r=0.4*.

Figure 18 illustrates the combined effects of the Prandtl number and dimemsionless frequency on the dimensionless pressure drop $\left|\lambda_b^*\right|$. The dimensionless pressure drop is a monotonic decreasing function of dimensionless frequency. Further, it decreases more rapidly when the Prandtl number assumes higher values. Figure 19 displays the influence of the heat generation/absorption parameter as well as dimensionless frequency on the dimensionless pressure drop $\left|\lambda_b^*\right|$. An increase in the heat generation/absorption parameter as well as dimensionless frequency reduced the dimensionless pressure drop. Also, the heat generation/absorption parameter considered is temperature dependent, and it is observed that as heat generation increases temperature also increases, though this growing trend is suppressed by larger Ω.

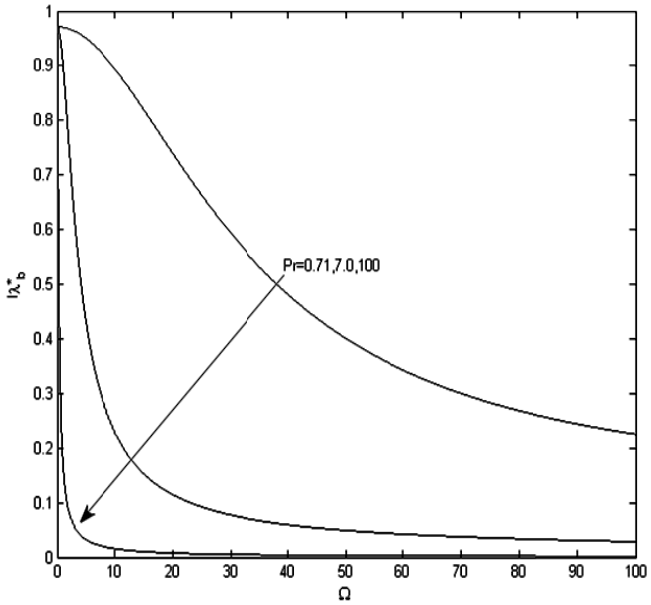

Fig.18. Distribution of $\left|\lambda_b^*\right|$ versus Ω for different values of Pr with *M=0.5*, $\beta_v Kn = 0.05$, *In=1.667*.

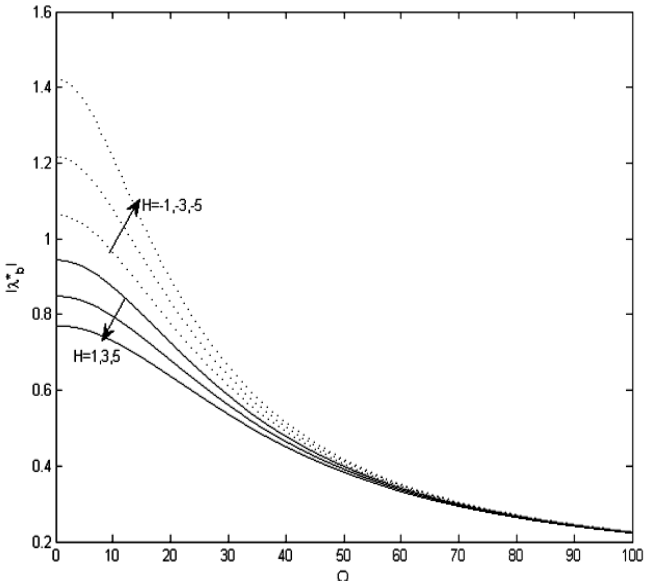

Fig.19. Distribution of $\left|\lambda_b^*\right|$ versus Ω for different values of H with *M=0.5*, β_v*Kn =0.05*, *In=1.667*.

Conclusions

A mixed convection flow of a heat generating/absorption fluid in the presence of Lorentz forces in a vertical micro circular subjected to a periodic sinusoidal temperature change at the surface is investigated. First-order slip and jump are taken into consideration. The solutions of the dimensionless velocity, temperature, pressure drop in terms of the magnetic field (M), heat generation/absorption parameter (H), fluid wall interaction parameter $(\ln)$, rarefaction parameter (Kn), Prandtl number $(\Pr)$, and the dimensionless frequency (Ω) were obtained. The main observations are pointed out below.

1. Increasing the value of the Lorentz force tends to slow down the movement of the fluid in the circular micro-duct for both small and large values of dimensionless frequency.
2. Heat absorption decreases the rate of heat transfer, whereas heat generation increases the rate.
3. The heat generation parameter produces acceleration in the convection flow, while the heat absorption parameter brings about retardation in the convection flow.
4. The oscillation amplitude of the dimensionless velocity has two local maxima, one close to the circular micro-duct axis while the other at the circular micro-duct for both large and small dimensionless frequency.
5. The impact of the heat generation parameter is suppressed by the growing dimensionless frequency (Ω)

Acknowledgments

The authors appreciate TETFUND for providing financial assistance to carry out this research.

Appendix

$$d_1 = I_0\left(0.5D_1\right) + \beta_v KnD_1 I_1\left(0.5D_1\right), \quad d_2 = \frac{D_1 d_1 - 0.5I_1\left(0.5D_1\right)}{8D_1 d_1},$$

$$d_3 = d_6 = I_0\left(0.5D_2\right) + \beta_v KnD_2 I_1\left(0.5D_2\right), \quad d_4 = I_0\left(0.5D_3\right) + \beta_v KnD_3 I_1\left(0.5D_3\right),$$

$$d_5 = \frac{1}{D_3^2 - D_2^2}, \quad d_7 = -\frac{1}{D_3^2 d_4}, \quad d_8 = -\frac{d_5 d_6}{D_3^2 d_4 \left\{I_0\left(0.5D_2\right) + \beta_v KnD_2 I_1\left(0.5D_2\right)\right\}},$$

$$d_9 = \frac{1}{\left\{I_0\left(0.5D_2\right) + \beta_v KnD_2 I_1\left(0.5D_2\right)\right\}\left\{D_3^2 - D_2^2\right\}}, \quad d_{10} = \frac{d_8}{D_3} 0.5 I_1\left(0.5D_3\right),$$

$$d_{11} = \frac{d_7}{D_3} 0.5 I_1\left(0.5D_3\right), \quad d_{12} = \frac{1}{8D_3^2}, \quad d_{13} = \frac{d_9}{D_2} 0.5 I_1\left(0.5D_2\right).$$

Nomenclature

$A(t)$ − function of time
B_0 − constant magnetic flux density
f − fanning friction factor
Gr − Grashof number
g − gravitational acceleration
H − dimensionless heat generation parameter
I_n − modified Bessel function of first kind and order n
i − imaginary unit
K_n − modified Bessel function of second kind and order n
Kn − Knudsen number, $\lambda/2R_0$
k − thermal conductivity
ln − fluid- wall interaction parameter, β_t/β_v
M − magnetic parameter
n − integer number
P − difference between the pressure and the hydrostatic pressure
Pr − Prandtl number
p − pressure
R − radial coordinate
$\Re$ − real part of a complex number
Re − Reynolds number
r − dimensionless radial coordinate
T − temperature
T_0 − mean temperature in a pipe section
T_1 − mean wall temperature
ΔT − amplitude of the wall temperature oscillations
t − time
U − fluid velocity
u − dimensionless velocity
u^* − dimensionless complex-valued function
u_a^*, u_b^* − dimensionless complex-valued function
X − longitudinal coordinate
α − thermal diffusivity
β − volumetric coefficient of thermal expansion
λ − dimensionless parameter

λ^* − dimensionless complex-valued function
λ_a^*, λ_b^* − dimensionless complex-valued function
η − dimensionless parameter
θ − dimensionless temperature
θ_a^*, θ_b^* − dimensionless complex-valued function
μ − dynamic viscosity
ν − kinematic viscosity
Φ − dimensionless heat flux
Φ_a^*, Φ_b^* − dimensionless complex-valued function
ρ − mass density
ρ_0 − mass density for $T = T_0$
τ_w − average wall shear stress
ω − frequency of the wall temperature oscillation
Ω − dimensionless frequency
σ − electrical conductivity of the fluid

References

[1] Arpaci V.S. and Larsen P.S. (1984): *Convection Heat Transfer*. − Prentice Hall Inc., Upper Saddle River.

[2] Baker I., Faw R.E. and Kulacki F.A. (1976): *Post-accident heat removal part I: heat transfer within an internally heated non-boiling liquid layer*. − Nucl. Sci. Eng., vol.61, pp.222-230.

[3] Chambre P.L. (1957): *Laminar boundary layer with distributed heat sources or sinks*. − Appl. Sci. Res. Sec. A4, 39.

[4] Chamkha A.J. (1999): *Hydromagnetic three- dimensional free convection on a vertical stretching surface with heat generation or absorption*. − Int. J. Heat Fluid Flow, vol.20, pp. 84-92.

[5] Foraboschi F.P. and Federico I.D. (1964): *Heat transfer in laminar flow of non-Newtonian heat generating fluids*. − Int. J. Heat Mass Transf. vol.7, pp.315.

[6] Modejski J. (1963): *Temperature distribution in channel flow with friction*. − Int. J. Heat Mass Transf. vol.6, pp.49.

[7] Ostrach S. (1952): *Laminar natural convection and heat transfer of fluids with and without heat sources in channels with constant with constant wall temperature*. − NASA Tech. Note 2863.

[8] Ostrach S. (1954): *Combined natural and force convection ow and heat transfer of fluids with and without heat sources in channels with linearly varying wall temperatures*. − NACA, TN 3141

[9] Ozisik M.N. (1993): *Heat Conduction*. − 2nd edn. Wiley, New York.

[10] Sparrow E.M. and Gregg J.L. (1960): *Newly quasi-steady free-convection heat transfer in gases*. − J. Heat Mass Transf. vol.82, pp.258-260.

[11] Jha B.K., Ajibade A.O. and Daramola D.A. (2014): *Mixed convection flow in a vertical tube filled with porous material with time-periodic boundary condition: steady-periodic regime*. − Afr. Mat. vol.26, pp.529-543.

[12] Jha B.K. and Ajibade A.O. (2009): *Free convective ow of heat generating/absorbing fluid between vertical porous plates with periodic heat input*. − Int. Commun. Heat Mass Transf. vol.36, pp.624-631.

[13] Jha B.K. and Aina Babatunde (2016*): Impact of heat generation/absorption on MHD mixed convection flow in a vertical tube having time periodic boundary condition: steady periodic regime*. − Heat Pipe Sci. Technol., vol.7, No.1-2, pp.123-147.

[14] Sparrow E.M. and Gregg J.L. (1960): *Newly quasi-steady free-convection heat transfer in gases*. − J. Heat Mass Transf. Trans. ASME Ser., vol.82, pp.258-260.

[15] Chung P.M. and Anderson A.D. (1961): *Unsteady laminar free convection*. − ASME J. Heat Mass Transf, vol.83, pp.473-478.

[16] Yang J.W., Scaccia C. and Goodman J. (1974): *Laminar natural convection about vertical plates with oscillatory surface temperature.* − Trans. ASME J. Heat Transfer, vol.96, pp.9-14.

[17] Nanda R.J. and Sharma V.P. (1963): *Free convection laminar boundary layer in oscillatory flow*. − J. Fluid Mech., vol.15, pp.419-428.

[18] Bar-Cohen A. and Rohsenow W.M. (1984): *Thermally optimum spacing of vertical natural convection cooled parallel plates*. − ASME J. Heat Transfer, vol.106, pp.116-123.

[19] Wang C.Y. (1988): *Free convection between vertical plates with periodic heat input*. − ASME J. Heat Transfer, vol.110, pp.508-511.

[20] Lage J.L. and Bejan A. (1993): *The resonance of natural convection in an enclosure heated periodically from the side.* − Int. J. Heat Mass Transfer, vol.36, pp.2027-2038.

[21] Antohe B.V. and Lage J.L. (1996): *Amplitude effect on convection induced by time periodic boundary conditions*. − Int. J. Heat Mass Transf., vol.39, pp.1121-1133.

[22] Kwak H.S., Kvwahara J.M. and Hyun J.M. (1998): *Resonant enhancement of natural convection heat transfer in a square enclosure*. − Int. J. Heat Mass Transf., vol.41, pp.2837-2846.

[23] Barletta A. and Zanchini E. (2002): *Time-periodic laminar mixed convection in an inclined channel*. − Int. J. Heat Mass Transf., vol.46, pp.551-563.

[24] Barletta A. and Rossi di Schio E. (2004): *Mixed convection flow in a vertical circular duct with time-periodicboundary conditions: steady-periodic regime*. − Int. J. Heat Mass Transfer, vol.47, pp.3187-3195.

[25] Makinde O.D. (2009): *Analysis of non-Newtonian reactive flow in a cylindrical pipe*. − ASME - Journal of Applied Mechanics, vol.76, 034502 (1-5).

[26] Chinyoka T. and Makinde O.D. (2012): *On transient flow of a reactive variable viscosity third-grade fluid through a cylindrical pipe with convective cooling*. − Meccanica, vol. 47, pp.667-685.

[27] Chinyoka T., Makinde O.D. and Eegunjobi A.S. (2013): *Entropy analysis of unsteady magnetic flow through a porous pipe with buoyancy effects.* − Journal of Porous Media, vol.16, No.9, pp.823-836.

[28] Singh G. and Makinde O.D. (2014): *Axisymmetric slip flow on a vertical cylinder with heat transfer.* − Sains Malaysiana, vol.43, No.3, pp.483-489.

[29] Jha B.K. and AinaBabatunde (2016): *MHD mixed convection flow in a vertical pipe with time periodic boundary condition: steady periodic regime*. − Int. J. Fluid Mech. Res., pp.350-367.

[30] Chen C.K. and Weng H.C. (2005): *Natural convection in a vertical microchannel*. − J. Heat Transfer, vol.127. pp.1053-1056.

[31] Jha B.K. and AinaBabatunde (2015): *Mathematical modelling and exact solution of steady fully developed mixed convection flow in a vertical micro-porous-annulus*. − Journal of Afrika Matematika, vol.26, pp.1199-1213.

[32] Sadeghi M., Sadeghi A. and Saidi M.H. (2014): *Gaseous slip flow mixed convection in vertical microducts of constant but arbitrary geometry*. − AIAA Journal of Thermophysics and Heat Transfer, vol.28, No.4, pp.771-784.

[33] Avci M. and Aydin O. (2009): *Mixed convection in a vertical microannulus between two concentric microtubes*. − J. Heat Transfer Trans. ASME 131: 014502.

[34] Sadeghi M. and Baghani M.H. Saidi (2014): *Gaseous slip flow mixed convection in vertical microducts with constant axial energy input*. − ASME Journal of Heat Transfer, vol.136, No.3, 032501.

[35] Weng H.C. and Jian S.J. (2012): *Developing mixed convection in a vertical microchannel*. − Adv. Sci. Lett. 5, pp.1-6.

[36] Jha B.K. and AinaBabatunde (2018): *Fully developed mixed convection flow in a vertical microtube with time periodic heating boundary condition.* − Multidiscipline Modeling in Materials and Structures, vol.14, No.4, pp.787-808.

Received: February 20, 2020

Revised: July 9, 2020